Identification of Orthotropic Plate Stiffness Using Open Hole Tensile Test

J. Molimard, R. Le Riche, A. Vautrin, and J. R. Lee, SMS/MeM, GDR CNRS 2519,
ENSM-SE, 158 Cours Fauriel, 42023 Saint Etienne, France

Abstract

Identification of mechanical parameters is still a challenge on real structures. With the improvement of optical full field measurement techniques, it becomes easier, but in spite of many publications showing the feasibility of such methods, experimental results are still scarce. We present here a first step towards a global approach of mechanical identification for composite materials. The chosen mechanical test is an open hole tensile test according to standard recommendations. For the moment, experimental data are provided by a moiré interferometry set-up. The global principle of the identification developed here is a minimization procedure, based on Levenverg-Marquardt agorithm. This approach has the advantage to have a high adaptability. In particular, the optical system and the signal processing can be modelized as well as the mechanical aspects. In the paper, different kind of cost functions are tested by using an identifiability criterion. Even if some mechanical considerations can be made, the simpler mathematical form is the more efficient. The used model is an analytical one based on Lekhnitskii approach. Identified values are similar to values from classical mechanical tests within 5 % except for the Poisson's ratio (15 %).

1. Introduction

Optical full-field method (OFFM) can be combined with theoretical analyses, based on an analytical model or finite element analysis to give rise to novel and efficient hybrid methods that can be useful to refine mechanical approaches of complex problems. In using reasonable criteria for the comparison between the two approaches, we can have both mechanical properties and a well-founded model. In this paper, we deal with an application related to the identification of mechanical properties. Extracting these parameters from the full-field maps requires the use of so-called inverse approaches such as model updating iteration, or the virtual fields method. The former strategy is more generic to obtain both a complete model and the mechanical properties; the parameters are adjusted in such a way that value computed with a model match the corresponding measurands, which are generally displacement or strain in OFFM-based tests [1,2]. When convergence is achieved with certain criteria, the final values are considered as the identified parameters.

The latter is a direct identification method. Therefore any model updating iteration is not necessary. This approach is also based on the processing of the heterogeneous strain fields. However in practice, it requires a well-chosen mechanical test to be conducted. The well-chosen test means an excitation of all strain components under the known boundary conditions, and hence, a T-shaped specimen under tensile loading [3], an unnotched specimen under Iosipescu shear test [4], and a thick laminate tube under compression [5] were proposed. By using these approaches, the mechanical properties can be identified, but it is difficult to provide a direct model for a tested complex structure. Further details about the virtual field method can be found in the recent publications reviewed systematically by Grédiac et al [6~8]. The identification strategy to be used in this study is a kind of model updating iteration method.

The aim of this paper is to determine the in-plane elastic properties of a thin orthotropic composite laminate coupon, namely the longitudinal Young's modulus E_{xx}, the transverse Young's modulus E_{yy}, the Poisson's ratio ν_{xy}, and in-plane shear modulus G_{xy}. For all elastic properties to be measured in a single test, the specimen must be designed in such a manner that all the strain components play a role in the response of the specimen. This is not as easy in practice as in theory, because due consideration must be taken with respect to the test apparatus and/or specimen geometry in the domain of mechanics. In this point of view, an open-hole tensile plate, proposed by Gardenas Garcia [9] is interesting. However, the heterogeneous strain fields are very localized near the hole thus experimental data are not easy to evaluate quantitatively with precision. Recently, the remarkable improvement in metrological qualities of OFFMs renders the open-hole tensile test a configuration of interest for the identification of material properties. Moreover, the plate with a hole is providing great services to many industrial applications; it brings about the merits of low cost, simplicity and easiness of repairing and joining between structural members. This is particularly so in the case of aerospace engineering. Finally, there is a known analytical exact solution, which becomes a convenience in the theoretical part of the identification strategy.

Using such a test, the choice of model updating is particularly efficient: geometrical aspects such as the hole center or geometry have to be known precisely (typically, the precision should be lower than $1/10^{th}$ of the hole diameter). Identification

procedure can include these parameters with mechanical ones. Last, the mechanical and material axis can be misaligned. Thus, a rotation angle has to be added for higher precision.

Many Optical Full Field Methods are available in the lab: grid method, image correlation, grating shearography, moiré interferometry, or speckle shearography. In a first step, we choose here to use the phase-shifting moiré interferometry due to its advantage of high spatial resolution and low sensitivity to spatial filtering.

3. Experimental conditions

3.1 Mechanical set-up

The specimen used for the open-hole tensile test is made of *Non-Crimped New Concept* (*NC2*®) developed by *Hexcel Composite* company. Chosen composite are made of very homogeneous planes of *Toray T700* 12K carbon fibres having $\boldsymbol{E_f}$= 240 GPa and an epoxy resin *RTM6*® having $\boldsymbol{E_m}$ =2.89 GPa; the corresponding fibre volume fraction is 50 %. Finally, the stacking sequence is $[\{0/90\}_3]_s$. Specimen geometry comes from recommendations given by aeronautic industry. The central hole has a diameter of 4 mm and the plate width is 26 mm. The thickness of the plate is 2 mm.

Experimental set-up is presented Figure 1. During the open-hole tensile test, a displacement was imposed on the movable jaw and the load was controlled using a classical load cell. The applied stresses for this open-hole tensile test were 6.1 MPa and 11.1 MPa.

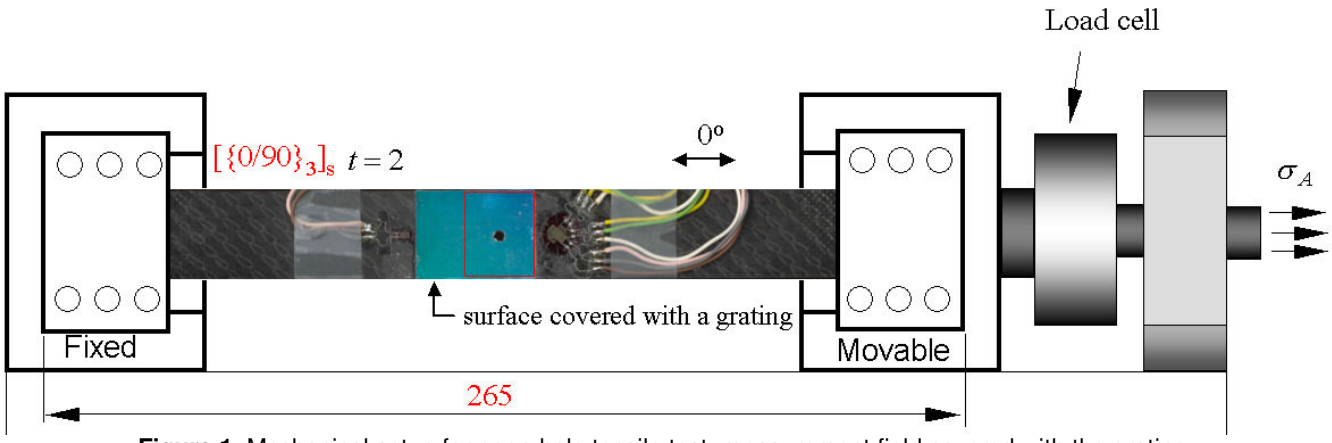

Figure 1. Mechanical setup for open-hole tensile test: measurement field covered with the grating

3.2 Phase-shifting moiré Interferometry

The optical arrangement of phase-shifting moiré interferometry is illustrated in Figure 2: a 150 mm-collimated beam obtained from a 10 mW He-Ne laser with a wavelength of 632.8 nm, a spatial filter and a collimating lens illuminates the three-mirror setup and the front surface of the specimen covered by a 1200 lines/mm diffraction grating. An opaque screen located in front of the collimating lens 1 switches the horizontal or vertical portion of beams. The fringe pattern in moiré interferometry is formed as a result of the interference on the optical grating of the two collimated beams of laser light.

Post, Han and Ifju and co-workers [10] carried out numerous developments related to the classical moiré interferometry, which were based on the intensity moiré fringe pattern. The idea behind the application of phase-shifting technique to moiré interferometry was first proposed by Kujawinska [11]. Practically, a glass plate is added on one beam. By rotating it, the optical path can be change, thus phase extraction is possible at any measurement point independently form the others.

Considering both the reference and deformed states, a difference in the optical path can be induced between the two diffracted beams at a given point. Consequently the phase determination of the moiré fringe pattern makes it possible to measure the ***u*** displacement, along the tensile direction ***x***.

$$u = \frac{p_s}{4\pi}\Delta\phi_h \tag{1}$$

Similarly the ***v*** displacement, along transverse direction ***y*** can be obtained as follows:

$$v = \frac{p_s}{4\pi}\Delta\phi_v \tag{2}$$

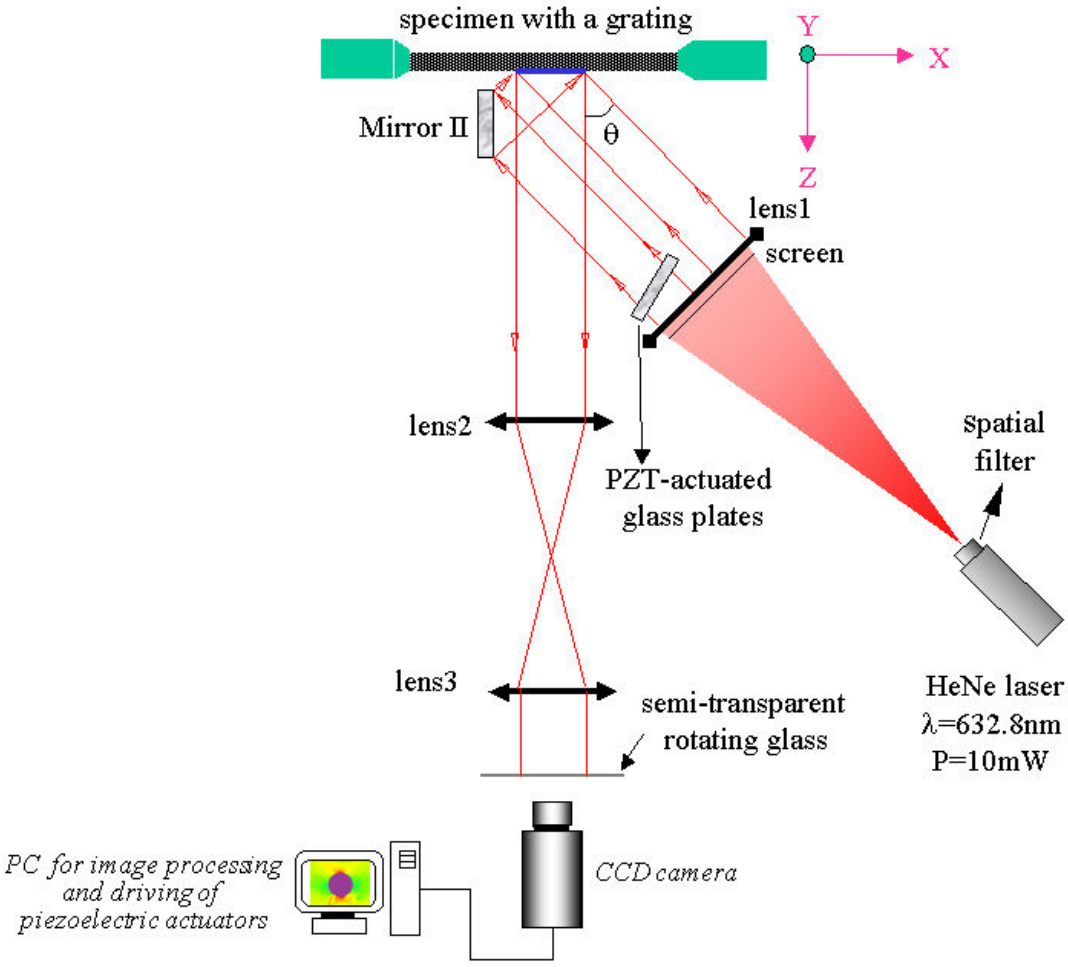

Figure 2. Optical arrangement of phase-shifting moiré interferometry.

where $\Delta\phi$ is the phase variation between reference and deformed state; the superscript represents respectively the horizontal (***h***) or vertical plane (***v***). A temporal phase-shifting algorithm was used for the quantitative phase determination of the acquired intensity fringe pattern. The used algorithm is the windowed discrete Fourier transform (WDFT) algorithm [11], where the phase shift (δ) is $\pi/3$ and one set is composed of eleven phase-shifted intensity samples.

Finally, a semi-transparent glass plate was the image plane, which is focused by lens 2 and 3. Through the rotation of the semi-transparent glass plate an optical temporal filtering was also carried out to remove the remaining speckle type noise. A 1296×1030 CCD camera with a high spatial resolution was selected to obtain an excellent initial spatial resolution. Finally, phase map were recorded using Frangyne® software from Techlab Company. Then, derivation from displacement to strain map is done by fitting a line on 7 pixels using a least square algorithm. Experimental data have the resolution of 20 με and a spatial resolution of 186.7 μm.

4. Theoretical model

The theoretical model is a solution proposed by Lekhnitskii [13] in the case of a hole on a thin plate of which dimensions (width and length) are considerably larger than the hole diameter. A uniform tensile stress is applied far from the hole. The general solution form is an infinite series, but classically, only one term is used; it has been proved to be enough in most cases. In a first step, this solution is implemented in the identification procedure. An analytical solution has some important advantages. Among them, the solution can be calculated at any experimental point, and the signal processing applied on experimental data can be very easily reproduced. Consequently, displacement derivations is performed by fitting a line over 7 pixels.

5. Identification strategy

As presented in Figure 4, the general scheme of our identification strategy consists of the three parts: an experimental OFFM, a theoretical model and an optimisation algorithm. The identification procedure was completed by minimizing the following function:

$$PI = \frac{1}{2n_p}\mathbf{R}^{\mathrm{T}}\mathbf{R} \tag{8}$$

where n_p is the number of effective data points in the measurement field and **R** is the vector with n_p residues. The form of the residue function will be discussed latter. As an example, the chosen one is written as follows:

$$R_{1,i}=R_i(E_{xx},E_{yy}G_{xy},\nu_{xy})=\sqrt{\left(\varepsilon_{xx,i}^{\exp}-\varepsilon_{xx,i}^{ana}\right)^2+\left(\varepsilon_{yy,i}^{\exp}-\varepsilon_{yy,i}^{ana}\right)^2+\left(\varepsilon_{xy,i}^{\exp}-\varepsilon_{xy,i}^{ana}\right)^2} \quad i=1,2\ldots n_p \tag{9}$$

The used minimisation algorithm was an improved Levenverg-Marquardt algorithm [14] and the improvements concern respect of parameter bounds and scaling. Details of its practical application can be found in Ref. [15] and the program developed in the reference was also used in this study.

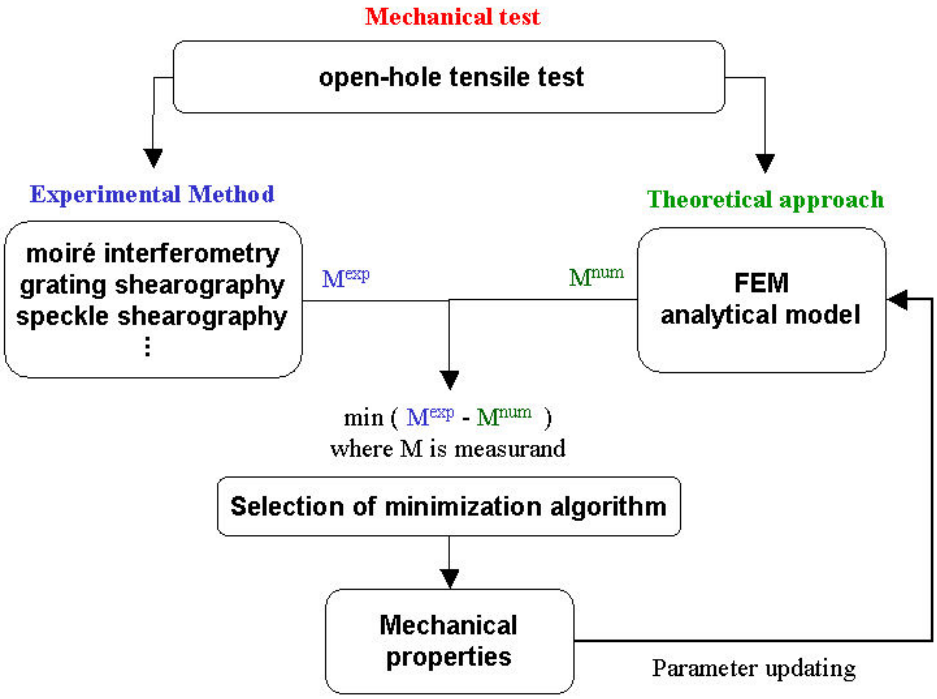

Figure 4. General scheme of hybrid methods based on OFFM and theoretical model.

6. Numerical simulation of the identification procedure

In order to verify the identification procedure, we have performed a numerical simulation of an open-hole tensile test. The composite material to be simulated is T300/976. The conditions of the numerical simulation and the in-plane properties of the material are given in Table 1. The in-plane strain maps obtained according to the simulation conditions are used instead of the experimental results. In the end of the identification program in Figure 5, we found the identified values, E_{xx} = 130 GPa, E_{yy} = 9.61 GPa, G_{xy} = 4.45 GPa, ν_{xy} = 0.29. The value of λ_{max} considered as convergence was 10^{10}, instead of infinity. In any parameters, errors in this simulation are less than 1 %, showing that no visible bias exist in this approach.

Some geometrical parameters have to be considered as parameters to be identified also such as the coordinates of the hole (x_o, y_o) and the two radii of the hole, considered to be elliptic (r_x, r_y) and a possible mechanical/material misalignment θ. In the same way, we found the identification values with respect to the eight parameters, x_o = 0.00, y_o = 0.00, r_x = 5.00 mm, r_y = 5.00 mm, θ = 0, E_{xx} = 130 GPa, E_{yy} = 9.64 GPa, G_{xy} = 4.465 GPa, ν_{xy} = 0.29. In any parameters, the errors in this case are also less than 1 %. These two examples show the capability of this identification procedure to recover the material and geometrical parameters.

In-plane properties of T300/976		Simulation condition	
Longitudinal Young's modulus (E_{xx})	130 GPa	Applied stress at infinity (σ_{xx})	5 MPa
		Hole position	(0,0)
Transverse Young's modulus (E_{yy})	9.65 GPa	Radius of hole	5 mm
		Plate section at infinity	200 mm^2
Shear modulus (G_{xy})	4.464 GPa	Increment for numerical differentiation	100 µm
Poisson's ratio (v_{xy})	0.29	Considered area for identification	(-75~85, -75~85) mm^2

Table 1. In-plane properties of the orthotropic material and the simulation conditions.

We next investigate various residue functions and explain why Eq. 9 has been selected as the final residue function. Including the residue function (***R1***) of Eq. 9, we present here three other residue functions. ***R2*** is based on a stress instead of strain. Then, normalization is performed using the first invariant. A residue function can also be defined only using the invariants (***R3***). This formulation should have the advantage of lesser sensitivity to axis misalignment. Last, the final residue function is an energy formulation (***R4***).

$$R_{2,i}=\sqrt{\frac{\left(\sigma_{xx,i}^{\exp}-\sigma_{xx,i}^{ana}\right)^2+\left(\sigma_{yy,i}^{\exp}-\sigma_{yy,i}^{ana}\right)^2+\left(\sigma_{xy,i}^{\exp}-\sigma_{xy,i}^{ana}\right)^2}{(\sigma_{1,i}^{ana})_2}} \tag{10}$$

where $\sigma_{1,i}=\sigma_{xx,i}+\sigma_{yy,i}$.

$$R_{3,i}=\sqrt{\left(\sigma_{1,i}^{\exp}-\sigma_{1,i}^{ana}\right)^2+\left(\sigma_{2,i}^{\exp}-\sigma_{2,i}^{ana}\right)^2+\left(\sigma_{3,i}^{\exp}-\sigma_{3,i}^{ana}\right)^2} \tag{11}$$

$$R_{4,i}=\sqrt{\left(\varepsilon_{xx,i}^{\exp}-\varepsilon_{xx,i}^{ana}\right)\left(\sigma_{xx,i}^{\exp}-\sigma_{xx,i}^{ana}\right)+\left(\varepsilon_{yy,i}^{\exp}-\varepsilon_{yy,i}^{ana}\right)\left(\sigma_{yy}^{\exp}-\sigma_{yy}^{ana}\right)+\left(\varepsilon_{xy,i}^{\exp}-\varepsilon_{xy,i}^{ana}\right)\left(\sigma_{xy,i}^{\exp}-\sigma_{xy,i}^{ana}\right)} \tag{12}$$

We compare the relative identification stability of these four residue functions by defining the identifiability: the first order Gauss-Newton approximation to Hessian matrix, $\widetilde{\mathbf{H}}=\nabla\mathbf{R}^T\nabla\mathbf{R}$ in the identification program gives a direction for searching the converged solution from the present step (*j*) to the next step (*j+1*). In this matrix, the influence of each parameter can be evaluated using the matrix's eigenvalues. Then, the identifiability factor should be defined as the maximum eigenvalue normalised by the minimum eigenvalue. Using the above definition, we investigate the four residue functions in the same way. The basic results are shown in Table 2. The residue function showing the best identifiability is the first one (***R1***). This is the reason why this function has been selected for the final identification procedure.

Residue function	Normalised identifiability factor		Characteristic of residue function
	4 parameters case	8 parameters case	
R_1	1	1	Reference case
R_2	1.69×10^2	5.87×10^6	Normalisation
R_3	3.45×10^2	1.10×10^4	Invariant form
R_4	2.40×10^2	1.82×10^2	Energy form

Table 2. Relative identifiabilities of various residue functions.

7. Results and discussions

A first identification is performed on experimental strain maps. The differences between the experimental and the analytical strain maps recalculated with the identified elastic constants are shown in Figure 5. The mean values of all the difference maps are close to zero. This implies that this identification procedure is also efficient in connection with the experimental results obtained by moiré interferometry of which resolutions were 20.4 με. No weakness on any difference strain map can be found. This shows that the residue function is well-balanced between the three experimental sets. Last, one should note that the difference maps underline the local effects due to stitching procedure used in NC2® technology. But, because it has been presented elsewhere[16], this point will not be developed in this paper.

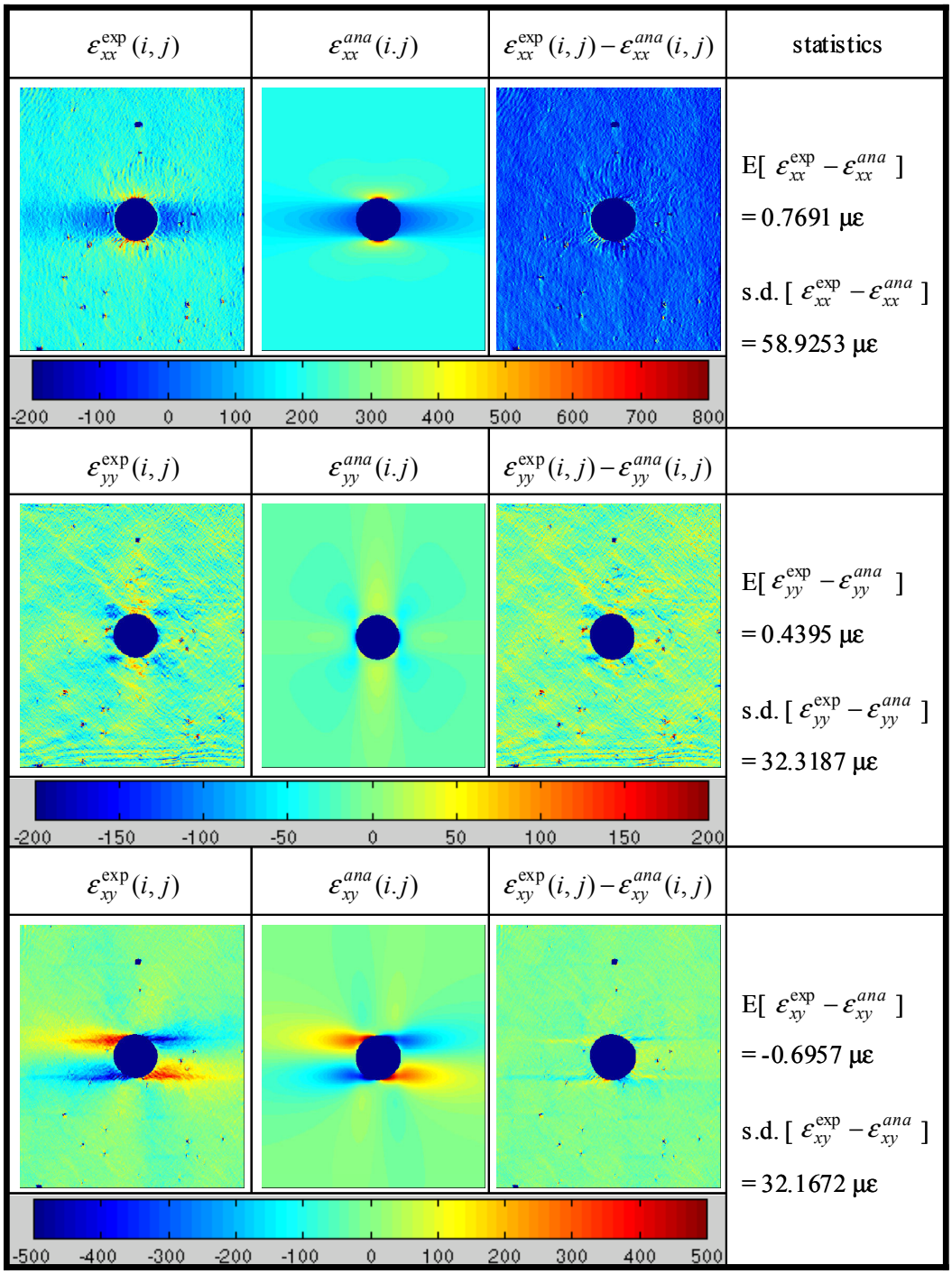

Figure 5. Differences between the experimental strain maps and the analytical strain maps recalculated with the identified elastic properties.

The first results are summed up in Table 3. They are compared to classical tensile tests using strain gages. Even if those tests are most commonly and widely used for estimating the elastic properties, strictly speaking, it is difficult to consider the values obtained by such tests as verified elastic properties because the heterogeneity gives rise to parasite effects that may cause unreliable results to be produced. We can consider them as merely reference values based on the usual tests. Anyway, the moiré interferometry based-identified values are found to agree within less than 5 % to the ESG-based reference values, with the exception of the Poisson's ratio. In general the two-dimensional reinforcement of the specimen shows very small Poisson's ratio. Therefore, in absolute terms, both results show to be almost zero, whereas in relative terms, they shows a difference of 26.5 %. Even if this explanation should be enough, it could be related to the model also: it is a first-order solution, and the width of the specimen is not at "infinity". This point has be investigated in the future.

	E_{xx}	E_{yy}	G_{xy}	ν_{xy}
Reference value	59.5 GPa	55.8 GPa	4.26 GPa	0.049
Identified value	57.1 GPa	58.1 GPa	4.48 GPa	0.062
Difference (%)	4.1%	4.0%	5.2%	26.5%

Table 3. Identified elastic constants of the biaxial *NC2* laminate.

8. Conclusion

This paper presents an iterative procedure for determination of the elastic properties of an orthotropic NC2® laminate. It is based on a normalized hole-on-plate tensile test. An identification procedure implies a lot of elements: optical full-field method, signal processing, theoretical approach, minimization algorithm, hence; in a first step, the conception of the identification system needs some arbitrary choices.

Here, experimental results comes from an in-plane sensitive phase-shifting moiré interferometry system because this method is the most sensitive available in the laboratory. The phase-shifting technique has made it possible to conduct quantitative and automated fringe analysis. Results appeared to be with a resolution of 20 με and a spatial resolution of 187 μm. The quality of the incoming signal allowed not to use any other signal processing than numerical derivation. In the future, other types of results should be investigated. In a practical point of view, speckle shearography should be a very interesting choice because of the no specimen preparing and the advantages of shearography, which are the optical derivation and its insensitivity to vibrations. But the use of such a technique implies the control of the signal processing *within the optimisation algorithm*.

As to the minimisation algorithm, a Levenverg-Marquardt algorithm with variable boundaries has been chosen. Even if the used method is a model updating iterative one, the identification strategy is simple and generic. Four cost functions are compared using an identifiability criterion, and the more stable is selected. This generic approach is very suitable for introducing signal processing capabilities.

Finally, the elastic parameters found with the identification procedure are close to results measured with 3 classical tensile tests and the difference is within the uncertainty range. Even if the Poisson's ratio values are very low, the difference on this parameter is quite different. It should be related to the theoretical model assumptions. This point will be investigated in a near future.

References

[1] F. M. Furgiuele, M. Muzzupappa, and L. Pagnotta, "A full-field procedure for evaluating the elastic properties of advanced ceramics," Experimental Mechanics, Vol. 37, 285-291 (1997).
[2] L. Bruno, F. M. Furgiuele, L. Pagnotta, and A. Poggialini, "A full-field approach for the elastic characterization of anisotropic materials," Optics and Lasers in Engineering, Vol. 37, 417-431 (2002).
[3] M. Grédiac, and F. Pierron, "A T-shaped specimen for the direct characterization of orthotropic materials," International Journal for Numerical Methods in Engineering, Vol. 41, 293-309 (1998).
[4] F. Pierron, and M. Grédiac, "Identification of the through-thickness moduli of thick composites from whole-field measurements using the Iosipescu fixture: Theory and simulations," Composite Part A, Vol. 31, 309-318 (2000).
[5] F. Pierron, S. Zhavoronok, and M. Grédiac, "Identification of the through-thickness properties of thick laminated tubes using the virtual field method," International Journal of Solids and Structures, Vol. 37, 4437-4453 (2000).

[6] M. Grédiac, E. Toussaint, and F. Pierron, “Special virtual fields for the direct determination of material parameters with the virtual fields method. 1-Principle and definition,” International Journal of Solids and Structures, Vol. 39, 2691-2705 (2002).
[7] M. Grédiac, E. Toussaint, and F. Pierron, “Special virtual fields for the direct determination of material parameters with the virtual fields method. 2-Application to in-plane properties,” International Journal of Solids and Structures, Vol. 39, 2707-2730 (2002).
[8] M. Grédiac, E. Toussaint, and F. Pierron, “Special virtual fields for the direct determination of material parameters with the virtual fields method. 3-Application to the bending rigidities of anisotropic plates,” International Journal of Solids and Structures, Vol. 40, 2401-2419 (2003).
[9] J. Gardenas Garcia, “Determination of the elastic constants using moiré”, Mechanical Research Communications, Vol. 27, No. 1, 69-77 (2000).
[10] D. Post, B. Han, and P. Ifju, “High sensitivity moiré: Experimental analysis for mechanics and materials,” Springer Verlag, New York (1994).
[11] M. Kujawinska, “Use of phase-stepping automatic fringe analysis in moiré interferometry,” Applied Optics, Vol. 26, 4712-4714 (1987).
[12] Y. Surrel, “Fringe analysis,” Photomechanics, P.K. Rastogi Ed., Springer Verlag, 55-102 (1999).
[13] S. G. Lekhnitskii, S. W. Tsai, and T. Cheron, “Anisotropic plates,” New York: Gordon and Breach 1968.
[14] F. Guyon, and R. Le Riche, “Least squares parameter estimation and the Levenberg-Marquardt algorithm: Deterministic analysis, sensitivities and numerical experiments,” Technical Report INSA de Rouen, No. 041/99, November 20 (2000).
[15] J. Molimard, and R. Le Riche, “Identification de piézoviscosité en lubrification,” Mécanique & Industries, Vol. 4, 645-653 (2003).
[16] J R Lee, J Molimard, A Vautrin and Y Surrel, Digital Phase-Shifting Grating Shearography for Experimental Analysis of Fabric Composites under Tension, Composite Part A: Applied Science and Manufacturing, Vol.35 (2004) To be published.